Elliptical isolated attosecond-pulse generation from an atom in a linear laser field

Xiaofan Zhang [ORCID],[1] Xiaosong Zhu,[2,*] Xi Liu [ORCID],[4] Feng Wang [ORCID],[1] Meiyan Qin,[1] Qing Liao,[1] and Peixiang Lu[3,†]

[1]*Hubei Key Laboratory of Optical Information and Pattern Recognition, Wuhan Institute of Technology, Wuhan 430205, China*
[2]*Wuhan National Laboratory for Optoelectronics and School of Physics, Huazhong University of Science and Technology, Wuhan 430074, China*
[3]*Guangdong Intelligent Robotics Institute, Dongguan 523808, China*
[4]*School of Physics and New Energy, Xuzhou University of Technology, Xuzhou 221018, China*

We theoretically demonstrate a scheme to produce elliptically polarized isolated attosecond pulses, based on the high-order harmonic generation from the current-carrying state of an atom exposed in linearly polarized laser fields. It is shown that the nonzero ellipticity of the attosecond pulse generated at the single-atom level is attributed to the nonvanishing angular momentum of the state, which is further elucidated by the strong-field approximation model. With specific carrier envelope phases (CEPs), isolated attosecond pulses with large ellipticity can be obtained. Moreover, the ellipticity of high-order harmonics remains almost invariable versus the CEP of the few-cycle driving field. Hence, the temporal profile and ellipticity of the attosecond-pulse radiation can be manipulated separately, which is beneficial to shape the attosecond-pulse radiation without compromising the ellipticity. The obtained elliptical attosecond pulse may serve as a potential tool to explore and manipulate the ultrafast dynamics in magnetic materials and chiral media.

I. INTRODUCTION

High-order harmonic generation (HHG) is a highly nonlinear phenomenon in interactions between matters and intense laser fields [1]. The HHG process can be understood by the three step recollision (TSR) model [2]: Under the influence of the driving field, the electron is ionized into the continuum, it is subsequently accelerated, and, finally, the photons with high energy are emitted when the electron recombines with the nucleus. The HHG has been a hot topic for its two fascinating applications: One is that the HHG is a useful tool to shed light on the internal structures and dynamical processes in atoms, molecules, solids, and plasmas on the attosecond time scale [3–11]; the other is that the HHG is an effective way to produce the attosecond laser pulse on a table-top scale facility [12–19].

In the latter case, the generation of linearly polarized attosecond pulses, both isolated attosecond pulses (IAPs) as well as regular pulse trains, has been paid much attention in most previous HHG works. In parallel with the linearly polarized attosecond pulses, the circularly or elliptically polarized attosecond pulses, which provide an additional degree of freedom, have abundant applications [20–23,29], such as the study of ultrafast chiral-specific dynamics in molecules [20] and x-ray magnetic circular dichroism spectroscopy [21,22]. Motivated by these important applications, some methods to produce such a light source have been proposed in many theoretical and experimental studies. Most of the scenarios can be separated into two types, i.e., by preparing the specified targets [24–27] and by designing two-dimensional (2D) synthesized driving fields [28–31]. In the former type of scenario, most works employ prealigned molecular targets. In this scenario, the ellipticity of high-order harmonics is not high [24–26]. Another special target, the state with angular momentum $|m| = 6$, has also been considered [27]. However, this target with such large angular momentum is rarely achieved in current experiments. According to the TSR model, the recollision probability of the electron based on the latter type of scenario drops dramatically. This results in a low conversion efficiency to high-order harmonics.

Recently, an experimental work using a 2D synthesized laser field, i.e., a counter-rotating bichromatic driving (CRBD) field, and a noble gas atom to deliver ultrashort quasicircular pulses in the extreme ultraviolet has emerged [31]. Using the CRBD driving field has been recognized as a promising technique to overcome the drawback mentioned above, i.e., low conversion efficiency. However, based on the selection rules [31,32], the generated high-order harmonic spectrum consists of double peaks with alternately left and right circular polarization [19–22,33–36,46]. The ellipticity of the synthesized attosecond pulses is reduced due to the opposite helicity harmonics. Additionally, the temporal profile and ellipticity of the attosecond pulse produced by the 2D synthesized driving field cannot be controlled separately. That is to say, when the driving field is changed to control the temporal profile of the attosecond-pulse radiation, e.g., to produce an IAP, the polarization of the harmonics is simultaneously changed and the ellipticity of the pulse radiation may decrease. Therefore, a scheme to efficiently generate elliptically polarized attosecond pulses and manipulate their temporal profile and ellipticity separately is still desired.

*zhuxiaosong@hust.edu.cn
†lupeixiang@mail.hust.edu.cn

In our paper, we demonstrate a scheme to produce an elliptically polarized isolated attosecond pulse, which is based on the HHG from the interaction between the linearly polarized few-cycle laser field and the current-carrying state of an atom target. It was generally assumed that the polarization of high-order harmonics from atoms is linear when the driving laser field is linearly polarized. This assumption originates from the fact that initial states with zero angular momentum were used in most works. Here, the polarization properties of the high-order harmonic emission are controlled by preparing the atomic state with the nonvanishing angular momentum. This atomic state has been demonstrated by employing circularly polarized pulses in theoretical and experimental works [37–39]. Although the linearly driving laser field is used, the high-order harmonics are elliptically polarized due to the nonvanishing angular momentum of the state. Moreover, when the carrier envelope phase (CEP) of the driving laser field is modulated, the ellipticity of the high-order harmonics is pretty much constant. Importantly, this result demonstrates that the temporal profile and ellipticity of the attosecond pulse can be manipulated separately.

II. THEORETICAL MODEL

The interaction between the linearly polarized laser field and the current-carrying state of the atom is described by the 2D single-active-electron time-dependent Schrödinger equation (TDSE) [40] [atomic units (a.u.) are used throughout this paper unless otherwise stated]:

$$i\frac{\partial}{\partial t}|\Psi(t)\rangle = H(t)|\Psi(t)\rangle, \quad (1)$$

in which $H(t)$ is the full Hamiltonian

$$H(t) = -\frac{1}{2}\nabla^2 + V(\vec{r}) + \vec{r} \cdot \vec{E}(t), \quad (2)$$

and the linear laser driving field $\vec{E}(t) = E_0 f(t) \cos(\omega t + \Delta\phi)\vec{e}_x$. E_0 and ω are the maximum amplitude and frequency of the pulse. $f(t)$ is the $\sin^2(\frac{\pi t}{T})$ envelope. $T = 3T_0$ is the full width at half maximum duration, where T_0 is the optical cycle of the ω field. $\Delta\phi$ is the CEP. $\vec{e}_x$ is the unit vector in the x direction. The atomic Coulomb potential is modeled by the 2D effective potential:

$$V(\vec{r}) = -\frac{Z(\vec{r})}{\sqrt{|\vec{r}|^2 + \alpha}}, \quad (3)$$

where $Z(\vec{r}) = 1 + 9\exp(-|\vec{r}|^2)$. The soft-core parameter $\alpha = 2.88172$ is used to obtain the ionization potential $I_p = 0.793$ a.u., which matches the first ionization potential of the Ne atom [19,41]. $\vec{r} \equiv (x, y)$ denotes the electron position in the two-dimensional x-y plane. The current-carrying states $2p_\pm$ with magnetic quantum numbers $m = \pm 1$, denoted by $|\phi_{2p_\pm}\rangle$, are obtained as $|\phi_{2p_\pm}\rangle = (|\phi_{2p_x}\rangle \pm i|\phi_{2p_y}\rangle)/\sqrt{2}$ [19], in which $|\phi_{2p_x}\rangle$ and $|\phi_{2p_y}\rangle$ are obtained through imaginary time propagation [42]. As a reference, we choose $Z(\vec{r}) = 1$ and $\alpha = 0.1195$ to obtain the 1s orbital with the same ionization potential. The angular momentum of the 1s orbital is zero. In the real time propagation, the time-dependent wave function $\Psi(\vec{r}, t)$ is obtained by solving the TDSE using the split-operator technique [40], and the time-dependent dipole acceleration can be obtained through the
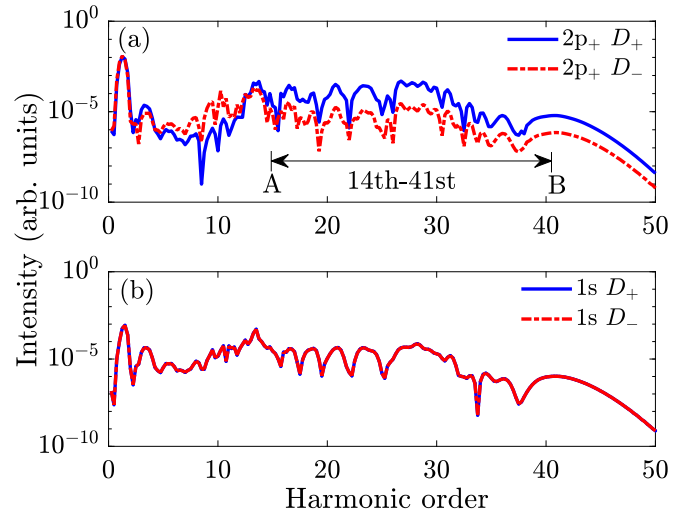
FIG. 1. High-order harmonic spectra from (a) the current-carrying state $2p_+$ of the model atom and (b) the reference 1s orbital. The blue solid and red dash-dotted lines represent the harmonic spectra for the right and left rotating components, respectively. The ionization threshold and cutoff position are labeled by A (14th-order harmonic) and B (41st-order harmonic) in panel (a). The wavelength of the driving laser is 800 nm and the intensity is 2×10^{14} W/cm^2. The CEP is $\Delta\phi = 0$.

Ehrenfest theorem:

$$\vec{q}(t) = -\langle\Psi(\vec{r}, t)|\nabla V(\vec{r}) - \vec{E}(t)|\Psi(\vec{r}, t)\rangle. \quad (4)$$

Then, the dipole acceleration in the frequency domain is calculated by $a_{x,y}(\Omega) = \int q_{x,y}(t)e^{-i\Omega t}dt$, in which Ω is the photon energy of the harmonics and subscripts x and y denote the corresponding x and y components. The harmonic radiation can also be divided into the left (a_-) and right (a_+) rotating components, which are obtained as $a_\pm = (a_x \pm ia_y)/\sqrt{2}$. The intensities of left and right polarized harmonic components are $D_\pm = |a_\pm|^2$. The ellipticity of harmonic radiation is calculated by $\epsilon = (|a_+| - |a_-|)/(|a_+| + |a_-|)$ [43,46]. In the following discussions, we take the current-carrying state $2p_+$ of the model atom as an example. The current-carrying state can be obtained with circularly polarized pulses propagating along the z axis [37,44]. It is worth nothing that the current-carrying state prepared in experiment is an ion state, which is different from the model atom used in our paper, while this model is still effective to study the important physics in the interaction between current-carrying states and strong laser fields and has been applied in previous works [45,46].

III. RESULTS AND DISCUSSIONS

The harmonic spectra from the $2p_+$ state driven by a linearly polarized laser field with the wavelength 800 nm and the intensity 2×10^{14} W/cm^2 are presented in Fig. 1(a). The reference spectra for the 1s initial state driven by the same laser field are also shown in Fig. 1(b). The left and right circularly polarized harmonic components are shown by the blue solid and red dash-dotted lines, respectively. From

Fig. 1(a), one can see that the intensities of the counter-rotating harmonic components $D_\pm$ are significantly different. Below the ionization threshold, the intensity of right rotating harmonics is higher than that of left rotating harmonics. At the plateau region AB (the 14th to 41st order), the intensity of left rotating harmonics becomes higher than that of right rotating harmonics. To demonstrate how large the influence of the nonvanishing angular momentum of the initial state is, we also present the counter-rotating harmonic spectra of the reference 1s orbital in Fig. 1(b). It is shown that the left and right rotating spectra are exactly the same, which indicates that the polarization state of the high-order harmonic radiation from the 1s orbital is linear. Comparing the results in Figs. 1(a) and 1(b), one can see that the angular momentum of the initial orbital plays an important role in the polarization state of the harmonic radiation.

It was generally assumed that the high-order harmonics from the atom are linearly polarized when the driving field is linearly polarized. This is indeed the case for the initial orbitals with zero angular momentum. However, if the initial orbital with nonvanishing angular momentum is applied, the situation becomes different. The mechanism of the high-order harmonics from such an initial orbital can be commonly understood by the TSR model. Because of the linearly polarized driving laser field, the ionized electron with zero initial transverse momentum, i.e., zero angular momentum, has the highest probability to recombine with its parent ion. That is to say, there is little contribution of the angular momentum to harmonics at the ionization or propagation step. So, the ellipticity of harmonics is mainly created at the recombination step, which can be demonstrated by the following simplified analysis in analogy to that in [27]. According to the strong-field approximation [47], the recombination dipole matrix element is calculated as $\vec{d} = \langle \Psi(\vec{r},0)|\vec{r}| \frac{1}{2\pi} \exp(-i\vec{k} \cdot \vec{r})\rangle$, in which $\Psi(\vec{r},0)$ is the wave function of the initial orbital and $\vec{k}$ is the recombination momentum. $\Psi(\vec{r},0)$ can be written as $f(r)e^{im\varphi}$ in cylindrical coordinates, in which φ is the azimuth angle. As the linear driving field is polarized along the x axis, $e^{-i\vec{k}\cdot\vec{r}}$ can be written as $e^{-ikr\cos\varphi}$. Applying the Bessel expansion $e^{-ikr\cos\varphi} = \sum_n (-i)^n e^{-in\varphi} J_n(kr)$ and denoting $B_n = \langle f(r)|r|J_n(kr)\rangle$, the x and y components of $\vec{d}$ are expressed as $d_x = \frac{1}{4\pi}(-i)^{m+1}[B_{m+1} - B_{m-1}]$ and $d_y = \frac{1}{4\pi}(-i)^{m+1}[iB_{m+1} + iB_{m-1}]$. The counterclockwise (+) and clockwise (−) components of $\vec{d}$ are $d_\pm = \mp\frac{\sqrt{2}}{4\pi}(-i)^{m+1}B_{m\mp1}$. Then the ellipticity can be expressed as $\epsilon = \frac{|B_{m-1}|-|B_{m+1}|}{|B_{m-1}|+|B_{m+1}|}$. If $m \neq 0$, either B_{m-1} or B_{m+1} dominates and the ellipticity ϵ is nonzero. The Bessel function satisfies the relationship $J_{-n}(kr) = (-1)^n J_n(kr)$. If $m = 0$, $|B_1| = |-B_{-1}|$ and the ellipticity is zero, which indicates that the high-order harmonics are linearly polarized. The analysis above indicates that the harmonic emission from the interaction between the linear driving field and the current-carrying state ($m \neq 0$) of the atom is elliptically polarized. Since the deviation above is generic, the elliptically polarized harmonic emission can be produced for any initial orbitals with $m \neq 0$ irradiated by linear drivers. In our paper, we choose the $2p_+$ state of the model atom with $m = 1$ as an example to demonstrate our scheme.
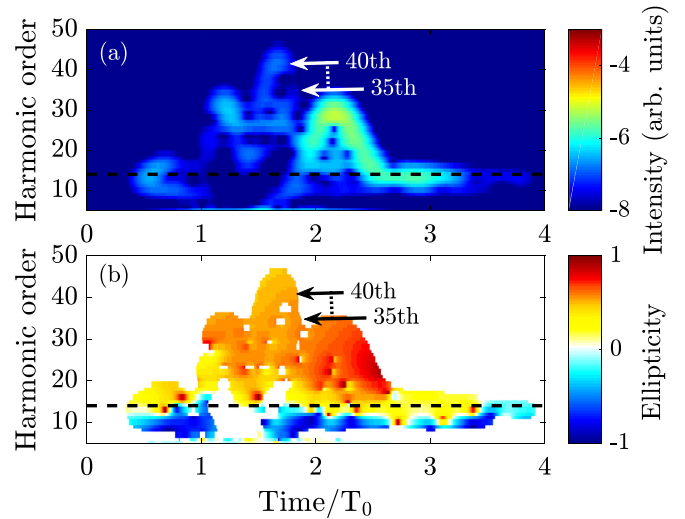
FIG. 2. (a) The intensity and (b) the ellipticity distribution of the harmonic emission from $2p_+$ state vs harmonic orders and emission time. The horizontal dashed lines mark the I_p. The laser parameters are the same as those in Fig. 1.

Next, in order to demonstrate our strategy, we calculate the harmonic intensity and ellipticity distributions using the Gabor transformation $\overrightarrow{\mathrm{GT}}(\Omega, t) = \frac{1}{\sqrt{2\pi}} \int dt \vec{q}(t) e^{-i\Omega t} e^{-(t-t_0)^2/(2\sigma^2)}$, where $\sigma = 3T_0$ [48]. The results are presented in Figs. 2(a) and 2(b), respectively. The horizontal dashed lines represent the ionization threshold. As shown in Fig. 2 (a), there are three dominant emission peaks above the ionization threshold. However, between the 35th and 40th order as labeled by the long and short white arrows, only the short trajectory in the second emission peak dominates. Consequently, harmonics in this range will support an IAP generation, which is discussed in Fig. 3 below. The ellipticity distribution is correspondingly presented in Fig. 2(b). One can see that, below the ionization threshold, the ellipticity is negative. Above the ionization threshold, the ellipticity of the emission peaks is positive, which is consistent with the result in Fig. 1(a), i.e., the intensity of left harmonics is higher than that of right harmonics. From Fig. 2(b), it is found that the ellipticity of the isolated emission peak between the 35th and 40th order as labeled by the long and short black arrows is more than 0.5. The results in Fig. 2 indicate that, with our scheme, an elliptically polarized IAP can be achieved by the harmonics between the 35th and 40th order.

Then, we present the synthesized attosecond pulse with elliptical polarization in the temporal domain in Fig. 3(a). The pulse is synthesized by the 35th to 40th harmonics for $\Delta\phi = 0$. Other laser parameters are the same as those in Figs. 1 and 2. As shown in Fig. 3(a), the pulse duration of the main isolated pulse is 622 as. For clearly showing the polarization characteristic of the attosecond pulse, the projection of the electric field onto the E_x-E_y plane is also plotted in Fig. 3(c), showing that the polarization of the radiated attosecond pulse is elliptical. The ratio of the minor axis to major axis of the electric field is 0.66, which indicates that the ellipticity of the
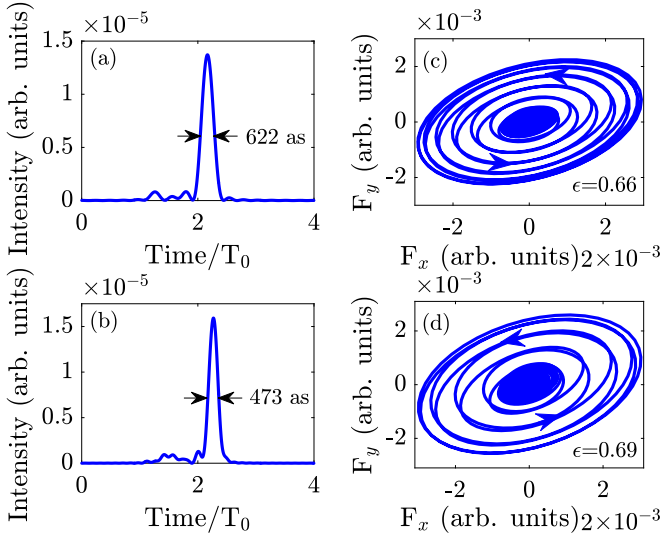
FIG. 3. (a), (c) Temporal profiles of the attosecond pulses synthesized by the harmonic spectra in the range of [38,49] orders for $\Delta\phi = 0$ and [29,38] orders for $\Delta\phi = 0.8\pi$. (b), (d) The electric fields of the attosecond pulses projected onto the F_x-F_y plane; the corresponding CEP and synthesized harmonic range are the same as those in panels (a) and (c), respectively. The arrows in the electric-field curves represent the direction of rotation. Other laser parameters are the same as those in Fig. 1.

attosecond pulse is 0.66. The rotating direction of the electric field is counterclockwise as labeled by arrows. We also present the elliptical IAP and the projection of its electric field onto the E_x-E_y plane for $\Delta\phi = 0.8\pi$ in Figs. 3(b) and 3(d). The pulse is synthesized by the 30th to 40th harmonics. From Fig. 3(b), the IAP can still be obtained, but the duration of the pulse is 473 as. It is shorter than that in Fig. 3(a) since the synthesized harmonic range is broader. The ellipticity of the electric field in Fig. 3(d) is 0.69, which does not change much comparing with that in Fig. 3(c). These results in Fig. 3 suggest that the elliptically polarized IAP can be produced from the current-carrying state of the atom driven by the linear laser field. Additionally, the duration of the IAP can be tuned by synthesizing different harmonic ranges at different CEPs, yet the ellipticity of the corresponding electric field remains basically invariable.

It has been reported that HHG and attosecond-pulse generation driven by few-cycle pulses would be primarily influenced by the CEPs [15,50–54]. Therefore, we further discuss the influence of the driving field CEP on the harmonic ellipticity and attosecond-pulse radiation. We present the harmonic ellipticity distribution as a function of CEP $\Delta\phi$ and harmonic order in Fig. 4(a). It is found that, below the ionization threshold labeled by the dashed line, the ellipticity is negative, that is, the harmonics are right elliptically polarized. Above the ionization threshold, the ellipticity is positive, i.e., the high-order harmonic emissions are left elliptically polarized. Moreover, the harmonic ellipticity is almost invariable versus the CEP of the driving field. That is to say, no matter what kind of temporal profile of the attosecond pulse is radiated, the ellipticity of the radiation is almost constant. This statement corresponds to the discussion above that the polarization state of the attosecond pulse relies on the initial orbital
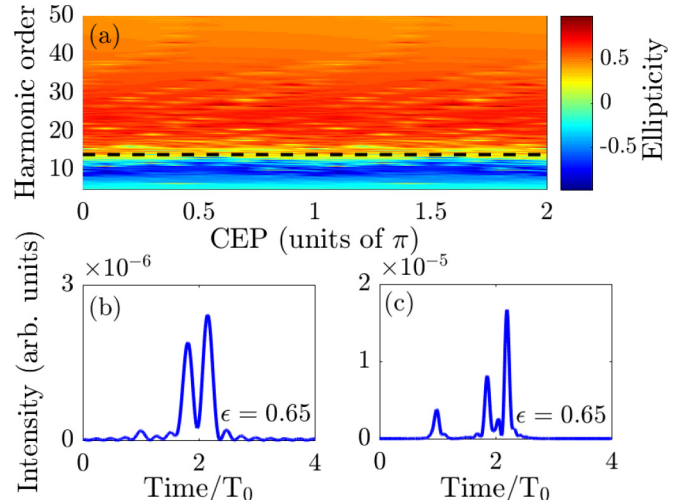
FIG. 4. (a) The ellipticity distribution of harmonic spectra vs harmonic order and CEP. (b), (c) Temporal profiles of the attosecond-pulse trains obtained by synthesizing [24,38] harmonic orders for the CEP $\Delta\phi = 0.1\pi$ and 0.3π. The ellipticity of all the pulse bursts is 0.65. The other laser parameters are the same as those in Fig. 1.

rather than the driving field. In Fig. 3, we have shown the synthesized IAPs with ellipticity 0.66 and 0.69 for $\Delta\phi = 0$ and 0.8π. Here, the generation of a regular attosecond-pulse pair and train with elliptical polarization is also demonstrated for $\Delta\phi = 0.1\pi$ and 0.3π. The results are presented in Figs. 4(b) and 4(c). From these two figures, one can see that there are two and three attosecond bursts generated, respectively. Additionally, these bursts are all elliptically polarized with almost the same ellipticity 0.65. Therefore, the results in Fig. 4 indicate that, although the temporal profile of the attosecond pulses obtained is strongly influenced by the CEP of the driving field, the polarization state of the attosecond pulses is almost the same.

IV. CONCLUSION

In conclusion, we have demonstrated a scheme to generate IAPs with large ellipticity from the interaction between the linear driving laser field and the current-carrying state of an atom. Our analysis has indicated that the ellipticity of the attosecond pulses originates from the nonvanishing angular momentum of the initial state. In addition, we have shown that, although the temporal envelope of the attosecond pulses can be tuned with the CEP of the few-cycle driving field, the ellipticity remains invariable. The temporal profile and the ellipticity of the attosecond pulses can be manipulated separately, which provides the possibility for pulse shaping without compromising the ellipticity of the attosecond pulse.

[1] F. Krausz and M. Ivanov, Rev. Mod. Phys. **81**, 163 (2009).

[2] P. B. Corkum, Phys. Rev. Lett. **71**, 1994 (1993).

[3] J. Itatani, J. Levesque, D. Zeidler, H. Niikura, H. Pépin, J. C. Kieffer, P. B. Corkum, and D. M. Villeneuve, Nature (London) **432**, 867 (2004).

[4] D. M. Villeneuve, Paul Hockett, M. J. J. Vrakking, and H. Niikura, Science **356**, 1150 (2017).

[5] S. Haessler, J. Caillat, W. Boutu, C. Giovanetti-Teixeira, T. Ruchon, T. Auguste, Z. Diveki, P. Breger, A. Maquet, B. Carré, R. Taïeb, and P. Salières, Nat. Phys. **6**, 200 (2010).

[6] P. M. Kraus *et al.*, Science **350**, 790 (2015).

[7] L. Li, P. Lan, L. He, W. Cao, Q. Zhang, and P. Lu, Phys. Rev. Lett. **124**, 157403 (2020).

[8] O. Smirnova, Y. Mairesse, S. Patchkovskii, N. Dudovich, D. Villeneuve, P. Corkum, and M. Y. Ivanov, Nature (London) **460**, 972 (2009).

[9] D. Shafir, H. Soifer, B. D. Bruner, M. Dagan, Y. Mairesse, S. Patchkovskii, M. Yu. Ivanov, O. Smirnova, and N. Dudovich, Nature (London) **485**, 343 (2012).

[10] J. Wu, M. Meckel, L. Ph.H. Schmidt, M. Kunitski, S. Voss, H. Sann, H. Kim, T. Jahnke, A. Czasch, and R. Dörner, Nat. Commun. **3**, 1113 (2012).

[11] P. Lan, M. Ruhmann, L. He, C. Zhai, F. Wang, X. Zhu, Q. Zhang, Y. Zhou, M. Li, M. Lein, and P. Lu, Phys. Rev. Lett. **119**, 033201 (2017); L. He, Q. Zhang, P. Lan, W. Cao, X. Zhu, C. Zhai, F. Wang, W. Shi, M. Li, X. Bian, P. Lu, and A. D. Bandrauk, Nat. Commun. **9**, 1108 (2018).

[12] P. M. Paul, E. S. Toma, P. Breger, G. Mullot, F. Augé, Ph. Balcou, H. G. Muller, and P. Agostini, Science **292**, 1689 (2001).

[13] G. Sansone, E. Benedetti, F. Calegari, C. Vozzi, L. Avaldi, R. Flammini, L. Poletto, P. Villoresi, C. Altucci, R. Velotta, S. Stagira, S. De Silvestri, and M. Nisoli, Science **314**, 443 (2006).

[14] J. Seres, V. S. Yakovlev, E. Seres, CH. Streli, P. Wobrauschek, CH. Spielmann, and F. Krausz, Nat. Phys. **3**, 878 (2007).

[15] E. Goulielmakis, M. Schultze, M. Hofstetter *et al.*, Science **320**, 1614 (2008).

[16] W. Boutu, S. Haessler, H. Merdji, P. Breger, G. Waters, M. Stankiewicz, L. J. Frasinski, R. Taieb, J. Caillat, A. Maquet, P. Monchicourt, B. Carre, and P. Salieres, Nat. Phys. **4**, 545 (2008).

[17] J. Li, X. Ren, Y. Yin, K. Zhao, A. Chew, Y. Cheng, E. Cunningham, Y. Wang, S. Hu, Y. Wu, M. Chini, and Z. Chang, Nat. Commun. **8**, 186 (2017).

[18] T. Gaumnitz, A. Jain, Y. Pertot, M. Huppert, I. Jordan, F. Ardana-Lamas, and H. J. Wörner, Opt. Express **25**, 27506 (2017).

[19] L. Medišauskas, J. Wragg, H. van der Hart, and M. Yu. Ivanov, Phys. Rev. Lett. **115**, 153001 (2015).

[20] A. Ferré, C. Handschin, M. Dumergue, F. Burgy, A. Comby, D. Descamps, B. Fabre, G. A. Garcia, R. Géneaux, L. Merceron, E. Mével, L. Nahon, S. Petit, B. Pons, D. Staedter, S. Weber, T. Ruchon, V. Blanchet, and Y. Mairesse, Nat. Photonics **9**, 93 (2014).

[21] O. Kfir, P. Grychto, E. Turgut, R. Knut, D. Zusin, D. Popmintchev, T. Popmintchev, H. Nembach, J. M. Shaw, A. Fleischer, H. Kapteyn, M. Murnane, and O. Cohen, Nat. Photonics **9**, 99 (2015).

[22] T. Fan *et al.*, Proc. Natl. Acad. Sci. USA **112**, 14206 (2015).

[23] I. Radu, K. Vahaplar, C. Stamm, T. Kachel, N. Pontius, H. A. Dürr, T. A. Ostler, J. Barker, R. F. L. Evans, R. W. Chantrell, A. Tsukamoto, A. Itoh, A. Kirilyuk, Th. Rasing, and A. V. Kime, Nature (London) **472**, 205 (2011).

[24] X. Zhou, R. Lock, N. Wagner, W. Li, H. C. Kapteyn, and M. M. Murnane, Phys. Rev. Lett. **102**, 073902 (2009).

[25] H. Niikura, N. Dudovich, D. M. Villeneuve, and P. B. Corkum, Phys. Rev. Lett. **105**, 053003 (2010).

[26] Anh-Thu Le, R. R. Lucchese, and C. D. Lin, Phys. Rev. A **82**, 023814 (2010).

[27] X. Xie, A. Scrinzi, M. Wickenhauser, A. Baltuška, I. Barth, and M. Kitzler, Phys. Rev. Lett. **101**, 033901 (2008).

[28] R. Shao, C. Zhai, Y. Zhang, N. Sun, W. Cao, P. Lan, and P. Lu, Opt. Express **28**, 15874 (2020).

[29] G. Lambert, B. Vodungbo, J. Gautier, B. Mahieu, V. Malka, S. Sebban, P. Zeitoun, J. Luning, J. Perron, A. Andreev, S. Stremoukhov, F. Ardana-Lamas, A. Dax, C. P. Hauri, A. Sardinha, and M. Fajardo, Nat. Commun. **6**, 6167 (2015).

[30] K. J. Yuan and A. D. Bandrauk, Phys. Rev. Lett. **110**, 023003 (2013)

[31] A. Fleischer, O. Kfir, T. Diskin, P. Sidorenko, and O. Cohen, Nat. Photonics **8**, 543 (2014).

[32] X. Liu, X. Zhu, L. Li, Y. Li, Q. Zhang, P. Lan, and P. Lu, Phys. Rev. A **94**, 033410 (2016).

[33] D. B. Milošević, Phys. Rev. A **92**, 043827 (2015); D. B. Milošević, W. Becker, and R. Kopold, *ibid.* **61**, 063403 (2000); D. B. Milošević, Opt. Lett. **40**, 2381 (2015).

[34] F. Mauger, A. D. Bandrauk, and T. Uzer, J. Phys. B **49**, 10LT01 (2016).

[35] D. D. Hickstein, F. J. Dollar, P. Grychtol, J. L. Ellis, R. Knut, C. Hernández-García, D. Zusin, C. Gentry, J. M. Shaw, T. Fan, K. M. Dorney, A. Becker, A. Jaroń-Becker, H. C. Kapteyn, M. M. Murnane, and C. G. Durfee, Nat. Photonics **9**, 743 (2015).

[36] K. M. Dorney, J. L. Ellis, C. Hernández-García, D. D. Hickstein, C. A. Mancuso, N. Brooks, T. Fan, G. Fan, D. Zusin, C. Gentry, P. Grychtol, H. C. Kapteyn, and M. M. Murnane, Phys. Rev. Lett. **119**, 063201 (2017).

[37] S. Eckart, M. Kunitski, M. Richter, A. Hartung, J. Rist, F. Trinter, K. Fehre, N. Schlott, K. Henrichs, L. P. H. Schmidt, T. Jahnke, M. Schöffler, K. Liu, I. Barth, J. Kaushal, F. Morales, M. Ivanov, O. Smirnova, and R. Dörner, Nat. Phys. **14**, 701 (2018).

[38] I. Barth and J. Manz, Phys. Rev. A **75**, 012510 (2007);

[39] A. Hartung *et al.*, Nat. Photon. **10**, 526 (2016).

[40] M. D. Feit, J. A. Fleck, Jr., and A. Steiger, J. Comput. Phys. **47**, 412 (1982).

[41] I. Barth and M. Lein, J. Phys. B **47**, 204016 (2014).

[42] X. B. Bian, Phys. Rev. A **90**, 033403 (2014).

[43] C. Chen, Z. Tao, C. Hernández-García, P. Matyba, A. Carr, R. Knut, O. Kfir, D. Zusin, C. Gentry, P. Grychtol, O. Cohen, L. Plaja, A. Becker, A. Jaron-Becker, H. Kapteyn, and M. Murnane, Sci. Adv. **2**, e1501333 (2016).

[44] T. Herath, L. Yan, S. K. Lee, and Wen Li, Phys. Rev. Lett. **109**, 043004 (2012).

[45] K. Liu, H. Ni, K. Renziehausen, J.-M. Rost, and I. Barth, Phys. Rev. Lett. **121**, 203201 (2018).

[46] X. Zhang, L. Li, X. Zhu, K. Liu, X. Liu, D. Wang, P. Lan, I. Barth, and P. Lu, Phys. Rev. A **98**, 023418 (2018).

[47] M. Lewenstein, Ph. Balcou, M. Ivanov, A. L'Huillier, and P. B. Corkum, Phys. Rev. A **49**, 2117 (1994).

[48] C. C. Chirilă, I. Dreissigacker, E. V. van der Zwan, and M. Lein, Phys. Rev. A **81**, 033412 (2010).

[49] X. Zhang, X. Zhu, X. Liu, D. Wang, Q. Zhang, P. Lan, and P. Lu, Opt. Lett. **42**, 1027 (2017).

[50] I. P. Christov, M. M. Murnane, and H. C. Kapteyn, Phys. Rev. Lett. **78**, 1251 (1997).

[51] F. Ferrari, F. Calegari, M. Lucchini, C. Vozzi, S. Stagira, G. Sansone, and M. Nisoli, Nat. Photonics **4**, 875 (2010).

[52] P. Lan, P. Lu, W. Cao, Y. Li, and X. Wang, Phys. Rev. A **76**, 011402(R) (2007).

[53] Z. Chang, Phys. Rev. A **70**, 043802 (2004).

[54] M. Hentschel *et al.*, Nature (London) **414**, 509 (2001).